

## Episodic Precambrian subduction

C. O'Neill<sup>a,\*</sup>, A. Lenardic<sup>a</sup>, L. Moresi<sup>b</sup>, T.H. Torsvik<sup>c,d,e</sup>, C.-T.A. Lee<sup>a</sup>

<sup>a</sup> Department of Earth Sciences, Rice University, United States

<sup>b</sup> Department of Mathematical Sciences, Monash University, Australia

<sup>c</sup> Centre for Geodynamics, NGU, Leiv Eirikssons vei 39, N-7491 Trondheim, Norway

<sup>d</sup> Institute for Petroleum Technology and Applied Geophysics, Norwegian University of Science & Technology, N-7491 NTNU, Norway

<sup>e</sup> School of Geosciences, Private Bag 3, University of the Witwatersrand, WITS, 2050, South Africa

Received 22 February 2007; accepted 5 April 2007

Available online 24 August 2007

Editor: C.P. Jaupart

### Abstract

The Precambrian geological record shows peak of activity at 1.1, 1.9–2.1, 2.7 and 3.5 Ga, often associated with massive crustal production, orogenesis and supercontinent cycles. It has been suggested that these bursts of tectonic activity are due to mantle avalanche events, where accumulating subducted slabs periodically penetrate the 670 km discontinuity, and subsequent upwelling counterflow and plume activity results in massive volcanism. Here we present paleomagnetic evidence for periods of rapid plate motions coinciding with the observed peaks in crustal age distribution. We present a new model for plate-driven episodic tectonics in the Precambrian, where higher mantle temperatures result in lower lithospheric stresses, causing rapid pulses of subduction interspersed with periods of relative quiescence. Plate-driven episodicity will naturally arise for hotter mantle temperatures of the early Earth and can explain rapid pulses of plate motion and crustal production without the need to invoke mantle avalanche events. © 2007 Elsevier B.V. All rights reserved.

*Keywords:* subduction; Precambrian tectonics; mantle convection; paleopoles

### 1. Introduction

The preserved crustal age distribution (McCulloch and Bennett, 1994; Condie, 2004) is a combination of contributions from juvenile crustal production, modification of older crust, and crustal recycling, modulated by the selective preservation of some continental regions such as cratons (McCulloch and Bennett, 1994; Stein and Hofmann, 1994; Condie, 2004) (Fig. 1). Of the preserved peaks in observed crust, 2.7 Ga and 1.9 Ga have, date,

been demonstrated to be associated with massive juvenile production as evidenced by Hf isotopes in zircons on many terranes (Condie, 2004; Kemp et al., 2006). Certainly earlier crustal production events contributed to most early–mid Archean crust, but this is not well constrained as most Archean terranes have been subject to heavy modification. The inferred crustal production rate during these events far exceeds the average crustal production rate for the Phanerozoic (Reymer and Schubert, 1984; Stein and Hofmann, 1994), and trace element distributions in sedimentary rocks indicate massive increases in the area of continental crust at these times (McClennan and Taylor, 1982; Taylor and McLennan, 1985). In addition, the progressive increase of  $\epsilon_{Nd}$  and Nb/Th through time indicates a bulk growth of crustal volume since the Archean

\* Corresponding author. Now at GEMOC ARC National Key Centre, Earth & Planetary Science, Macquarie University, Sydney, NSW, 2109, Australia.

E-mail address: [coneill@els.mq.edu.au](mailto:coneill@els.mq.edu.au) (C. O'Neill).

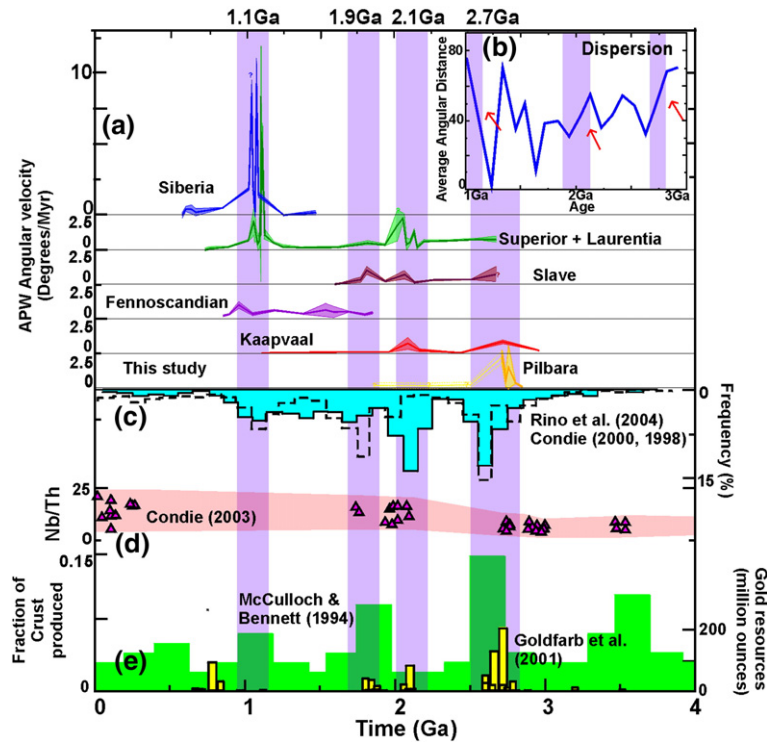


Fig. 1. (a) Apparent polar wander (APW) angular velocities vs time for seven stable Precambrian terranes over which good data coverage exists (Table 1). Uncertainty regions are shaded. Note that the each province has been staggered at  $1^\circ$  intervals for clarity. Statistically significant peaks in the APW velocities at 1.1, 2.1 and 2.7 Ga indicate rapid plate motions at these times. Question marks denote poles whose ages are contested. These poles are not critical to our conclusions. (b) Average angular distance of our APW paths vs time. Large changes in the average angular distance between poles at 1.1,  $\sim 2.1$ –1.9 and 2.7 Ga (red arrows) suggest motion between plates, rather than true polar wander, is responsible for the peaks in APW velocity observed in (a). (c) Distribution of U/Pb zircon ages from juvenile continental crust (Dotted line: (Condie, 1998, 2003); Filled histogram (Rino et al., 2004), showing peaks in preserved continental crust at discrete intervals. (d) Nb/Th vs age for oceanic basalts and komatiites (purple diamonds, from Condie (2003)). Nb/Th is used as a proxy for Nb/U, due to the mobility of U, and reflects the successive depletion of the mantle through time. (e) Age distribution of the continental crust in 200 Myr intervals (green histogram, from McCulloch & Bennett (1994)), and orogenic gold reserves vs time (gold histogram, from Goldfarb et al. (2001a,b)). The crustal age distribution reflects crustal preservation, which is a function of recycling and production rates through time. Goldfarb et al. (2001a,b) note that orogenic gold resources likely reflect crustal preservation through time, however, the distribution also suggests massive orogenesis at the time of their formation. (For interpretation of the references to colour in this figure legend, the reader is referred to the web version of this article.)

(McCulloch and Bennett, 1994; Collerson and Kamber, 1999; Condie, 2003), and  $^{40}\text{Ar}$  and  $^{18}\text{O}$  constraints argue against massive crustal recycling into the deep mantle (Coltice et al., 2000; Simon and Lécuyer, 2005), supporting the contention that juvenile crustal production is episodic.

On top of this juvenile crustal production signature is the record of crustal modification commonly associated with massive orogenesis accompanying supercontinent assembly — or at least the collision and dispersal of discrete continental blocks. 2.7 Ga probably saw the assembly of a late Archean supercontinent. Laurentia, Baltica and Siberia show evidence for major collisions in the interval 2.725–2.680 Ga (Condie, 2004), and Western Australia and Africa have collisional records between 2.680 and 2.650 Ga (Aspler and Chiarenzelli, 1998;

Condie, 2004). At 2.1 Ga, most terranes show evidence of rifting which Condie (2004) attributes to the breakup of the late Archean supercontinent, though West Africa and Amazonia show evidence for collisions during this time. The anomalous tectonic activity of the 2.1–1.9 Ga interval culminated with major collisions between Laurentia, Baltica and Siberia at 1.85 Ga — associated with a burst of juvenile crustal production (Condie, 2004). 1.1 Ga saw the formation of the supercontinent Rodinia with major collisions evidenced on most terranes (Torsvik, 2003).

Most of our evidence for these times is from cratons — renowned for their tenacity and perhaps not representative of average crust in the past. It has been suggested that the process of cratonization itself requires special geodynamic scenarios, such as times of vigorous plume activity (Griffin et al., 1999), or subduction of buoyant oceanic

lithosphere (Snyder, 2002; Lee, 2006). The temporal correlation between juvenile crustal production and cratonization suggests common tectonic circumstances.

Episodic behaviour has exerted a first-order effect on the geological record and mantle evolution, and it is important to understand its ultimate cause. Both the supercontinent cycle and juvenile crustal production can be considered responses to the tectonic and mantle regimes during these times, and the question we address in this study is what was the global tectonic regime during these remarkable events?

These periods of activity have been attributed to mantle avalanche events, where the dynamic layering of the mantle, induced by the spinel  $\rightarrow$  perovskite + magnesio-wüstite phase transition at 670 km periodically breaks down, and a catastrophic breakthrough of slabs occurs in a short-lived period of whole mantle convection. This hypothesis predicts an increase in plume activity associated with these overturns — supported by Nd and Sr isotope ratios of many juvenile terranes (Stein and Hofmann, 1994), and also provides a scenario for the cratonization of these terranes. Other alternatives have been put forward to explain this episodicity, such as superplumes (Condie, 2003).

Here we explore another hypothesis: namely that increased mantle heat production in the Precambrian resulted in decreased mantle viscosities, affecting the coupling between the plates and the convecting mantle, thus resulting in the breakdown of continuous plate tectonics. Analysis of magnetic anomalies in ocean basins indicate that, for the past 180 Myr, seafloor spreading has been a remarkably continuous, smooth process (Müller et al., 1997), and this has come to be regarded as a characteristic of plate tectonics (Richards et al., 2001). However, this might not have been the case in the Precambrian. A number of workers have explored scenarios for lid-driven episodicity, including Turcotte (1993) for transient thermal boundary layer convection on Venus, and van Thienen et al. (2004) for episodic dynamics associated with the eclogite transition in subducting slabs. Alternatively, Moresi and Solomatov (1998) explored regimes of mantle convection with a temperature-dependent viscosity and brittle failure. They showed that for weak plates (i.e. low yield strength) the mantle is in a mobile-lid regime where the lithosphere participates in convective overturn. Plate tectonics is an example of mobile-lid convection. For a much stronger lithosphere (higher yield stress) the lithosphere can resist convective stresses, and convection occurs in a stagnant lid regime, where the hot, convecting interior is overlain by a rigid, strong, immobile lithosphere. Intermediate between these regimes, however, is an episodic regime, where long periods of

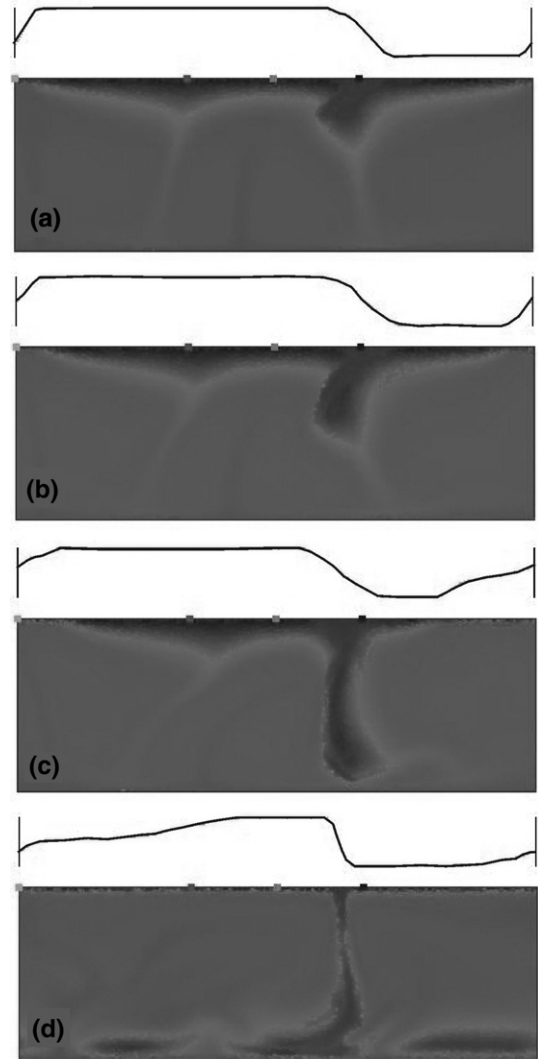


Fig. 2. Episodic mantle overturn for a basal Rayleigh number of  $10^7$ , internal heating production of  $2 \times 10^{-11}$  W/kg, with a viscosity contrast of  $10^5$  across the mantle. The depth scale is 670 km, and the temperature contrast is 2000 K. Normalised velocity at each timestep is shown as horizontal profile. Simulations performed using the finite-element particle-in-cell code Ellipsis (Moresi et al., 2003) on a  $128 \times 256$  grid, assuming a viscoplastic rheology with a lithospheric yield strength of 25 MPa. A strain-weakening was included in this example also, to localise plastic deformation. Free-slip top and bottom boundaries were used, and reflective side boundaries. Times shown are 2, 4, 7, and 10 Myr. Stagnant lid convection thins the lithosphere beneath upwelling and thickens it beneath downwellings (top). The combination of viscous traction forces from the convecting mantle and gravitational buoyancy forces combine to break the viscoplastic lid (middle). This is rapidly recycled in a burst of vigorous plate motion. Convection resumes under a thin, viscous stagnant lid which grows thicker with time.

quiescence (essentially stagnant lid convection) are interspersed by episodes of rapid subduction and overturn. An example is shown in Fig. 2. The transition

from mobile to episodic convection depends on the ratio of lithospheric strength to convective stresses. Moresi and Solomatov (1998) explored the yield conditions under which a lithosphere would be mobile or episodic, suggesting that greater lithospheric strength on Venus might give rise to episodic subduction. For an Earth-like plate strength, it would be useful to know the mantle conditions under which the mobile-lid regime breaks down. The most obvious difference between the present-day mantle and that of the past is its thermal state, in particular the effect of increased radiogenic heat production in the mantle in the past.

The approach of this paper will be two-fold. First we will assess the evidence for plate-driven episodicity in the Precambrian. In particular, paleomagnetic data are sensitive to rapid excursions in plate motion, and we will determine if there is evidence for such events in the past. Secondly, we present a robust modelling suite showing what happens to plate-tectonic like systems when internal heat generation is turned up. We will determine the parameter range over which the transition from plate tectonics to episodic convection occurs, and assess the plausibility of this mechanism in the Precambrian.

## 2. Approach and methodology

### 2.1. Paleomagnetic data

Paleomagnetic data provide important constraints on surface motions during these events but Precambrian paleomagnetic data is inevitably of lower quality than for the Phanerozoic. In particular, Precambrian apparent polar wander (APW) paths are sporadically sampled, over long time periods, and so are likely to represent a minimum-motion curve. APW paths represent the apparent motion of the rotation axis relative to the continent depending on whether one plots the movement of the north or south pole. Precambrian pole polarity is ambiguous and we therefore carefully constructed APW paths so that the distance between consecutive poles was minimized; this also leads to a minimum-motion curve. We constructed APW paths for seven Precambrian terranes over which sufficient data of reasonable quality exists, and which span a significant portion of time (Table 1). The APW paths do not directly reflect the motion of plates, due to sparse sampling, but do give a minimum constraint on the velocity of the plates over time.

Uncertainty regions for our APW velocities are determined from the combined percentage errors of  $A95/(\text{angular distance between poles})$  and  $\Delta t/\text{age}$  ( $A95$  is the nominal uncertainty value for paleopole positions, being the 95% confidence interval of the position of the

pole in degrees). Further details concerning data selection are provided in Table 1. Sparse sampling between data points will also result in lower APW velocity estimates than the true amount, a considerable problem with early (Archean) data. The uncertainty regions for the data are valid if the uncertainties in the system are succinctly encompassed by  $A95$  and the age uncertainties, i.e. there are no unquantified systematic uncertainties.

### 2.2. Numerical modelling of mantle convection

We model mantle convection using a well-established finite element/lagrangian integration point code (Ellipsis, Moresi et al. (2003)). The code solves the standard convection equations, i.e. Stokes equation for infinite Prandtl number subject to the incompressibility constraint, coupled with the energy equation including an internal heating term. The simulations we present are non-dimensional, but the results have been scaled using appropriate temperature, depth and viscosity scales for Earth's mantle.

Our initial starting point is a convecting system with a basal Rayleigh number of  $10^7$ , a Frank–Kamenetski style temperature-dependent viscosity which varies over 5 orders of magnitude (equivalent to an activation energy of  $\sim 200$  kJ/mol in the Arrhenius formulation, see Reese et al. (1999), and a simple homogenous yield stress (i.e. a uniform yield stress, with no depth-variation), which we vary. In addition to a temperature drop (which results in a significant thermal boundary layer at the base of the upper mantle), we also incorporate internal heat generation, which we vary to simulate mantle conditions in the Precambrian. The internal heat production, together with the yield stress, form our primary variables.

## 3. Results and discussion

### 3.1. Paleomagnetic results

We have plotted the angular velocity of each APW path against time in Fig. 1. Three major peaks in APW angular velocity are evident, at 1.1, 1.9–2.1 and 2.7 Ga. The magnitude of these excursions are discernible above the estimated uncertainties in the data. It should be noted that some data, denoted by question marks, are of dubious quality and are included in Fig. 1 for illustrative purposes only, and not essential to our primary results. The individual data points are discussed in the footnote to Table 1. In particular, the older portions of the Slave are considered unreliable, particularly with respect to ages, and the 2.7 Ga event is not, given the published data, robust in the Slave. It is, however, apparent on both the Pilbara and Kaapvaal terranes, and probably real. The

Pilbara data are not considered reliable for younger ages, but the average background APW velocities are included for illustration. The 2.1–1.9 Ga events, which are considered related (Condie, 2004), are evident on the Kaapvaal, Slave and Superior/Laurentia cratons, though significant evidence at 1.9 Ga is primarily from the Slave, either due to poor sampling elsewhere, or else due to the more localised nature of the later stages of this event. The excursions at 1.1 Ga, particularly on the Siberian and Superior/Laurentia cratons, are well sampled, and have been previously identified (Evans, 2003). The magnitude of these events is dependent on the sampling — the dense sampling at 1.1 Ga probably explains the relative magnitude of this event compared to the older velocity excursions. The low APW velocities between events is not, however, solely due to sparse sampling; the excursions exist for paths with similar sampling before, during, and after these events.

Two possible explanations exist: extremely rapid plate motions during these intervals, or rapid motion of geographic, and subsequently magnetic pole (True Polar Wander, TPW (Evans, 2003)).

It is difficult to distinguish rapid plate motion from TPW signatures in the Precambrian paleomagnetic record. Indeed, rapid plate motions and subduction can cause a significant re-distribution of density anomalies within the Earth, leading to TPW, so the two mechanisms may at times be related. One potential way to differentiate between these two processes, though not unique, is to determine the dispersion of these poles, as shown in Fig. 1b. The dispersion of the poles is determined by interpolating the APW paths at 10 Myr intervals, and calculating the average angular distance between poles. For TPW events without associated plate motion, the plate themselves may not move significantly, so the dispersion of poles should not be largely effected. In

#### Notes to Table 1:

We used data from the Global Paleomagnetic Database, and other sources (listed below). To ensure significant data quality, we selected only data with a demagnetization code of 3 or higher, and an A95  $\sim <15$ . To ensure reliable dates we only used data since the mid-eighties where possible, and with an age-uncertainty of generally less than  $\pm 100$  Myr, though these constraints are relaxed for periods of little data. We imposed a smoothness constraint on our APW paths to avoid unrealistic jerks caused by sampling of poles close together in time. Bold A95 denotes use of A95 uncertainties rather than  $\alpha_{95}$ . Bold age uncertainties denote use of nominal uncertainties for these points. Anabar and Aldan Shields combined in Fig. 1. Italicized entries are considered not reliable, and are either not included in final analysis, or marked with the symbol “?” in Fig. 1 for illustrative purposes. GPD reference number: Global paleomagnetic database (McElhinny, M.W. and Lock, J. (1996). IAGA paleomagnetic databases with Access, *Surv. Geophys.*, 17, 575–591).

S2003: Strik, G., Blake, T.S., Zegers, T.E., White, S.H., Langereis, C.G. (2003) *Journal of Geophysical Research. B. Solid Earth*, doi:10.1029/2003JB002475.

H2004a: Hanson, R.E., Crowley, J.L., Bowring, S.A., Ramezani, J., Gose, W.A., Dalziel, I.W.D., Pancake, J.A., Seidel, E.K., Blenkinsop, T.G., and Mukwakwami, J. (2004). Coeval large-scale magmatism in the Kalahari and Laurentian cratons during Rodinia assembly: *Science*, 1126–1129 DOI: 10.1126/science.1096329.

H2004b: Hanson, R.E., Gose, W.A., Crowley, J.L., Ramezani, J., Bowring, S.A., Bullen, D.S., Hall, R.P., Pancake, J.A. & Mukwakwami, J. (2004). Paleoproterozoic intraplate magmatism and basin development on the Kaapvaal Craton: Age, paleomagnetism and geochemistry of  $\sim 1.93$  to  $\sim 1.87$  Ga post-Waterberg dolerites. *S. African J. of Geology*, 53–74.

S2006: 2006 Letts S. & Torsvik, T.H. (manuscript in prep.)

W1999: Walderhaug, H.J., Torsvik, T.H., Eide, E.A., Sundvoll, B. & Bingen, B. (1999), *EPSL* 169, 71–83.

MT2003: Meert, J.G. & Torsvik, T.H. (2003), *Tectonophysics* 375, 261–288.

P2003: Pesonen, L. J.; Elming, S.-A.; Mertanen, S.; Pisarevsky, S.; D’Agrella-Filho, M. S.; Meert, J. G.; Schmidt, P. W.; Abrahamsen, N.; Bylund, G. (2003), *Tectonophysics*, 375, 289–324.

B2000: Buchan, K.L., Mertanen, S., Park, R.G., Pesonen, L.J. Elming, S.A., Abrahamsen, N. Bylund, G. (2000), *Tectonophysics* 319, 167–198.

MS1998: Smethurst, M.A., Khramov, A. & Torsvik, T.H. (1998), *Earth Sci. Rev.* 43, 1–24.

W2006: Weil, A.B., Geissman, J.W., Ashby, J.M. (2006), A new paleomagnetic pole for the Neoproterozoic Uinta Mountain supergroup, Rocky Mountain States, USA, *Precambrian Research* 147, 234–259.

YH2000 *Yoshihara & Hamano (2000) Phys. Earth & Planet. Int.* 117, p295.

<sup>P</sup> Data represent magnetic overprint and thus ages are speculative — included only to illustrate typical APW rate outside the 2.7 Ga event.

<sup>a</sup> Carbonate ages from the Siberian platform are included because they are constrained stratigraphically, and bounded by volcanic units, despite poorly determined individual ages. Their inclusion is not critical to the APW spike at 1.1 Ga, it exists even if the carbonate poles are removed.

<sup>b</sup> The age of the Kapuskasing dykes has been recently criticized since it is only constrained by an Ar/Ar age. Criticism or alternate age not yet published. Its inclusion is not crucial to the APW excursion at 1.9–2.1 Ga, the event occurs above the level of the uncertainties even if the pole is removed.

<sup>c</sup> Listed as Marathon Reverse (Fort Francis) in the GPD.

<sup>d</sup> Not included in this study due to contested age, new ages unpublished.

<sup>e</sup> Retained due to lack of coverage  $\sim 2.7$  Ga, though age should be viewed as extremely dubious. Without this pole the Slave demonstrates a decline in APW velocities from  $\sim 2.7$  Ga until 2.1 Ga.

Table 1  
Paleopoles used to construct APW velocities for Fig. 1

Sample	Age (Ma)	+/- (Myr)	Latitude	Longitude	$\alpha_{95}$
<i>Pilbara</i>					
HP2 <sup>P</sup>	1700	>100	-25.3	211.9	3
Mt. Tom Price <sup>P</sup>	2000	>100	-37.4	220.3	11.3
MT7-10 <sup>P</sup>	2207	>100	-53.2	203.9	5.3
P8-10 S2003	2715	2.5	-59.1	186.3	6.1
P4-7 S2003	2736	15.5	-50.4	138.2	12.5
P2 S2003	2766	2	-46.5	152.7	15.2
P1 S2003	2772	2	-40.8	159.8	3.7
Millindinna Complex GPD1278	2860	20	-11.9	161.3	5.2
<i>Kaapvaal</i>					
Umkondo Diabase Sills H2004a	1108	<b>Range 1106–1112</b>	61.1	38.5	<b>4.9</b>
Umkondo Sills H2004	1108	<b>Range 1106–1112</b>	55.4	37.6	<b>10.6</b>
Waterburg Group Intrusions H2004b	1875	<b>Range 1879–1872</b>	15.6	17.1	<b>8.9</b>
Bushveld S2006	2059	1	18.4	31.8	2.1
Gamagara GPD3553	2130	70	2.2	81.9	9.2
Ongeluk Lavas GPD3175	2222	13	-0.5	100.7	6.6
Mbabane Pluton GPD2391	2687	6	19.7	105.7	12
Derdepoort Basalt GPD3432	2782	5	39.6	184.7	10.4
Nelshoogte Pluton GPD3184	3179	18	-17.6	129.8	13
<i>Fennoscandia</i>					
Hunnendalen Dykes W1999	848	27	-41	222	6
Mean Baltica MT2003	930	2	-43	213	<b>5</b>
Mean Baltica MT2003	975	30	-1.4	234.7	<b>17</b>
Mean Baltica MT2003	1120	20	3	217	<b>15</b>
Mean Baltica P2003	1266	5	4	158	<b>4</b>
Mean Baltica P2003	1512	20	39	171	<b>16</b>
Mean Aland dolerite B2000	1567	5	20	185	<b>37</b>
SE quartz porphyry dykes B2000	1618	2	30	175	<b>6</b>
Mean Baltica P2003	1770	<b>20</b>	42	221	<b>7</b>
Mean Baltica P2003	1840	<b>20</b>	48	225	<b>3</b>
Mean Baltica P2003	1878	3	41	233	<b>5</b>
<i>Siberia (Aldan Shield)</i>					
Baikalia Sediments MS1998	590	20	56.5	359	6
Lena River Redbeds GPD3301	615	35	54	348.2	9.2
Ust-Kirbinskaya Suite MS1998	650	20	58.1	355	9
Kandykskaya Suite GPD3518	975	25	59.4	176.5	5
Sette-Daban Sills P2003	1005	4	0	177	2
Nelkan & Ignican GPD3476 <sup>a</sup>	1012.5	12.5	57.6	219.5	12.3
Milkon Formation GPD3476 <sup>a</sup>	1025	40	57.6	196.1	5.5
Kumakha Formation GPD3476 <sup>a</sup>	1040	55	58.9	201.2	7.8
Malgina Formation P2003 <sup>a</sup>	1043	14	58.3	230.5	2.9
<i>Siberia (Anabar Shield)</i>					
Kessyusa Formation GPD3164 <sup>a</sup>	540	5	37.6	345	12.8
Sukhotungusinskaya GPD3028 <sup>a</sup>	1040	60	-7.8	225.3	6.5
Linok Formation GPD3355 <sup>a</sup>	1067.5	32.5	-15.2	256.2	5.5
Chieress Dyke GPD3345	1384	2	4	258	9
Kuonamka Dykes P2003	1503	5	6	234	28
<i>Laurentia + Superior</i>					
Brock Inliner Sills MT2003/GPD1876	723	3	-2	165	16
Franklin Dykes MT2003/GPD222	723	3	9	152	5
Uinta Mtn Supergroup W2006	775	25	0.8	161.3	4.6
Tsezotene Sills MT2003/GPD1875	778	2	-2	138	5

(continued on next page)

Table 1 (continued)

Sample	Age (Ma)	+/- (Myr)	Latitude	Longitude	$\alpha_{95}$
<i>Laurentia + Superior</i>					
Upper Little Dal MT2003/GPD1884	778	2	24	159	11
Little Dal A+B MT2003	780	<b>20</b>	-9	140	11
Tsezotene Fm. MT2003/GPD1291	780	<b>20</b>	12	1148	8
Haliburton Intrusions MT2003/GPD7116	980	50	-36	143	6.3
Jacobsville SS Mean MT2003/GPD1111	1050	50	-9	183	4.5
Freda Sandstone MT2003/GPD1060	1058	8	1	180	5.9
Nonesuch Shale MT2003	1060	<b>20</b>	10	177	7.8
Clay-Howells Carb. MT2003/GPD2518	1075	15	27	179	7
Lake Shore Traps MT2003/GPD536/2247	1087	2	22	181	5.9
Portage Lake Lavas MT2003/GPD236/2247	1095	3	27	181	2.6
Upper Osler volcanics MT2003	1098	<b>20</b>	34	178	10
Mean Logan Dykes MT2003	1100	<b>20</b>	35	181	10
Keewawanaw N+R dykes MT2003/GPD1102	1102	<b>20</b>	44	197	11
Logan Sills MT2003/B2000	1108	<b>1</b>	49	220	3
Coldwell Complex MT2003/GPD2529	1108	<b>1</b>	49	200	16.5
Seabrook Lake Carb. MT2003/GPD2587	1113	<b>36</b>	46	180	11
Abitibi Dykes MT2003/GPD2773	1141	<b>1</b>	44	211	9.8
Sudbury Dykes B2000	1235	<b>4</b>	-3	192	3
Mackenzie Dykes B2000	1267	<b>2</b>	4	190	5
St. Francois Mtn B2000/P2003	1476	<b>16</b>	-13	219	7
Superior craton Case A mean pole P2003	1767	<b>27</b>	-11	272	27
Molson Dykes C2 P2003/GPD3342	1877	<b>4</b>	28.7	216	5.6
Minto Dyke Swarm P2003/GPD3204	1998	<b>2</b>	38.2	173.8	11
Kapuskaing Dykes GPD2501 <sup>b</sup>	2043	14	61.3	253	11.9
Marathon Reverse Pol dykes GPD3061 <sup>c</sup>	2076.5	4.5	51.2	174.7	6.8
Molson Dykes C1 GPD3061	2091	2	53	180	6.2
Marathon Normal GPD3061	2124.5	10.5	42.7	195.8	6.3
Molson B Dykes GPD3258	2145	25	27.1	219.2	2.6
Biscotasing Dykes GPD2771	2166.5	1.5	27.8	223.3	4.5
Maguire Dykes GPD3204	2236.5	27.5	-8.5	266.6	8.3
Matachewan Dykes GPD2487	2454	2	46.5	50.5	2.9
Pikwitonei Granulite GPD3258	2665	25	20.9	226.4	6.5
Red Lake Gr.stn. belt Batholiths GPD2751	2715	15	75	222	16
<i>Slave</i>					
Seton GPD1147	1600	100	25	263	7
Kahochella GPD1867	1700	50	14	270	5
Dogrib GPD240	1750	50	7	282	9
Kahochella GPD1867	1800	30	-7	298	10
Seton GPD1147	1830	10	2	267	7
Duck Lake GPD240	2050	50	-6	313	17
Indin GPD240	2093	86	19	284	8
Caribou Lake GPD1651	2186	10	14	296	5
Easter Island GPD1651	2350	150	-32	338	5
8a YH2000	2656	14	49.1	136.8	13.2
<i>Dogrib2 GPD240<sup>d</sup></i>	2692	80	35	130	4

reality, some dispersion occurs due to the different latitudes of the sampling sites during TPW. Significant variations in pole dispersion, however, may indicate rapid motion of the plates with respect to one another, particularly if the dispersion occurs for poles of similar paleolatitudes. The magnitudes of the variations in pole dispersion at 1.1, 2.1 and 2.7 Ga, together with dis-

persions variations for poles with similar paleolatitudes, suggest that the large variations in APW angular velocity at these times have rapid plate motion as a significant contribution. This does not rule out TPW during these events, which in any case, as noted above, is expected to accompany an episodic subduction event, but does strongly suggest plate motion is a significant factor.

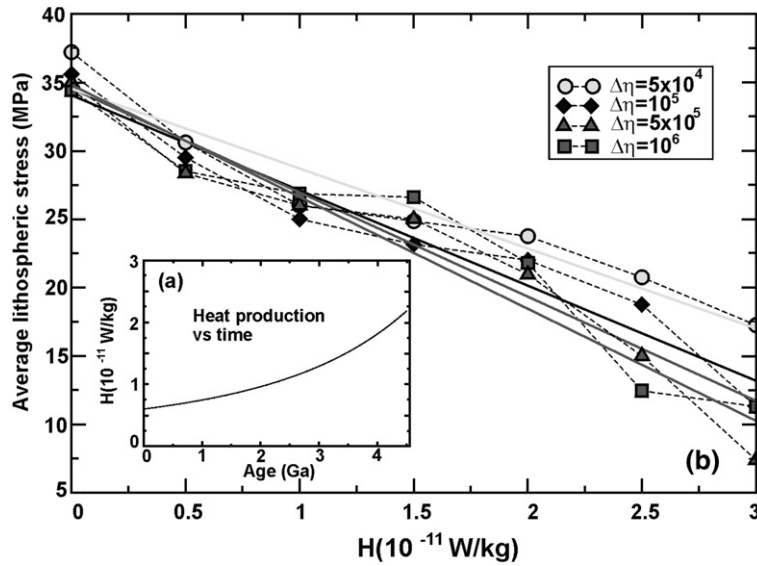


Fig. 3. (a) (inset) Mantle heat production vs time, for  $^{238}\text{U}$ ,  $^{235}\text{U}$ ,  $^{40}\text{K}$  and  $^{232}\text{Th}$ , for the present-day concentrations and half-lives listed in Turcotte and Schubert (1982). (b) Average lithospheric stress (MPa) vs internal heat production for stagnant lid convection with a basal Rayleigh number of  $10^7$ , on a  $128 \times 128$  grid for a variety of viscosity contrasts ( $\Delta\eta$ ) across the mantle.

### 3.2. Geodynamic modelling results

Fig. 3a illustrates the change in mantle heat production through time as a consequence of the decay of the main heat-producing elements (HPEs) in the mantle, namely  $^{235}\text{U}$ ,  $^{238}\text{U}$ ,  $^{232}\text{Th}$  and  $^{40}\text{K}$ . Higher concentrations of these isotopes in the past would have led to an increase in mantle heat production of a factor of 6 over 4.55 Ga (Turcotte and Schubert, 1982). The variation in heat production strongly influences mantle temperatures, but how does this affect plate-driving forces? Convective stresses ( $\tau$ ) induced on a thermal boundary layer are a product of velocity ( $v$ ) and viscosity ( $\eta$ ) (Turcotte and Schubert, 1982), i.e.:

$$\tau \sim v\eta/\delta \quad (1)$$

where  $\delta$  is the velocity length scale. Increases in internal heat production will increase the internal Rayleigh number and thus convective velocities, potentially increasing the convective stresses. However, the increase in internal temperatures will also lower the viscosity, decreasing the convective stresses. Which of these effects is dominant depends on the temperature-dependence of viscosity, and the Rayleigh number. For a strongly convecting system with a strongly temperature-dependent rheology, like the Earth's mantle, the relative change in velocity will be small compared to the drastic drop in interior viscosity. This effect is shown in Fig. 3b for the stagnant lid case, for a range of viscosity con-

trasts. The simulations in all cases are for constant values of heat production, and run to a statistical steady state. Different simulations at different heat production values encompass the range expected for Earth's history (Fig. 3a).

In the Precambrian, convective stresses would be lower than at present and may fall below the level required for continuous plate tectonics. Instead the planet may exhibit episodic plate tectonics. This regime is in many ways similar to that postulated for Venus today (Moresi and Solomatov, 1998). Fig. 4a illustrates the transition in tectonic regime for increasing mantle heat production. Fig. 4b maps the transition from mobile-lid to episodic convection for a range of lithospheric yield strengths and internal heat production values. The transition from mobile to episodic convection will occur for increasing heat production (Stein et al., 2004) or, as noted by (Moresi and Solomatov, 1998) increasing lithospheric yield strength. We note that for high yield strengths, increasing the internal heat production may cause a decrease in convective stresses to significantly below the plate's intrinsic strength, and under these conditions convection may be in a stagnant lid.

This work predicts strongly time-dependent subduction under the hotter mantle conditions of the Precambrian. This is a different mechanism from previous work on episodic Precambrian behaviour (Turcotte, 1993; Stein and Hofmann, 1994; van Thienen et al., 2004), as it is dependent only on the mechanical coupling of the

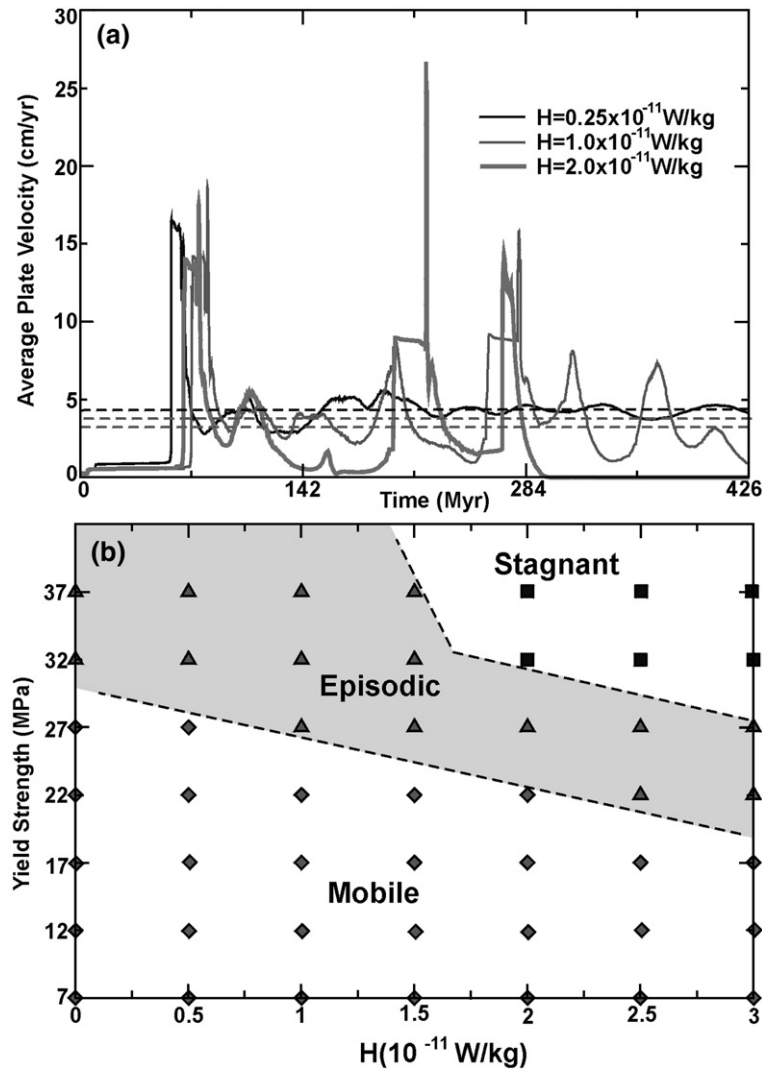


Fig. 4. (a) Average surface velocity vs time for heat production of values of 0.5, 1.0 and  $2 \times 10^{-11} \text{ W/kg}$ , for a constant lithospheric yield strength in this example of 27 MPa. Decrease in convective stress results in extremely time-dependent to episodic tectonics for higher mantle heat production. (b) Tectonic regime in yield-strength — heat production space. The effective yield strength of a plate is likely to be significantly less than that estimated for dry rock experiments (Kohlstedt et al., 1995), and the range of 10–30 MPa is the effective plate strength, i.e. the strength of the weakest portions of the plate which are most likely to fail (eg. fault zones), and is consistent with modelling large-scale deformation (Beaumont et al., 2004), subduction initiation (Hall and Gurnis, 2005), transform motion (Zhong et al., 1998; Tackley, 2000; Hall and Gurnis, 2005), stress drops during earthquakes (Kanamori, 1994), and rock experiments with significant pore pressure (Kohlstedt et al., 1995) and on altered rock (Escartin et al., 2001). For our preferred range (18–30 MPa), increase in mantle heat production in the past is likely to result in an episodic mantle convection regime.

plates and mantle. The simulations are run to a statistical steady state, so numerous overturns occur in each simulation as shown in Fig. 4a. The time period between overturns is sensitive to yield stress, mantle structure, and the work-balance between the driving mantle and the plate, but is typically between 200 Myr and 1 Gyr. The velocity during the overturn events is up to 25 cm/yr (Fig. 4a) — compared with (minimum) APW velocities on the Superior of nearly 15 cm/yr, the magnitudes agree well. An important caveat to these results is the validity

of our simple uniform yield stress to represent the rheology of plates. A uniform yield stress is the simplest representation of plate strength that allows mobile-lid behaviour, and as such is the most sensible starting point for an exploration of the plate–mantle coupling through time, though ideally further work would explore the robustness of our results to more complicated rheologies. The absolute values of yield stress used here are between 18 and 30 MPa — any higher than this and we do not get mobile-lid convection for present-day

conditions for our mantle configuration. These values are consistent with previous modelling and other constraints (see Fig. 4), and predict a transition into episodic convection for mantle heat production values typical of the Precambrian.

Pulses of rapid subduction would result in massive arc-volcanism, and continental growth by arc-accretion — thus this mechanism predicts synchronous continental growth and fast plate velocities (cf. Fig. 1). Many lines of evidence suggest a subduction origin to at least some continental formation events (Calvert et al., 1995; Lee, 2006). Massive orogenesis is expected to accompany the subduction pulses, as observed in the geological record of many cratons (Calvert et al., 1995; Condie, 2004), and required for the distribution of large orogenic gold deposits during these times (Goldfarb et al., 2001a,b). These subduction episodes would also cause major upwelling counterflow, and invigorate plume formation if slabs descended to the core–mantle boundary, contributing to major surface volcanism. Intracrustal melting observed on many cratons occurs generally 50–100 Myr after derivation of juvenile crust from the mantle (McClennan and Taylor, 1982; Taylor and McLennan, 1985). If this intracrustal melting is due to basaltic underplating by plumes, then the timescale is of the same order as we predict between subduction pulses/crustal formation and surface plume activity. This mechanism also explains the combined plume/subduction signatures in many of these juvenile crustal formation events.

Mantle avalanche events may have similar consequences to episodic subduction, particularly if slabs penetrating the lower mantle are contiguous with surface plates. Irrespective of avalanches however, this work shows that Precambrian subduction may not be in steady state. Archean tectonics would not just be a faster version of plate tectonics, but rather a fundamentally different regime characterized by episodic bursts of subduction and tectonic activity.

#### 4. Conclusions

The paleomagnetic analysis of this paper shows large variations in APW velocities at certain times in the Precambrian. These APW velocity excursions coincide with episodes of crustal production, and are best explained by large variations in average plate velocities at these times. TPW may also contribute to these signals, but the dispersion of paleopoles during these events suggests a strong relative plate motion component. The two primary mechanisms for fast plate motion are either mantle avalanche events, which has been previously postulated, or episodic Precambrian subduction, as put forward here.

Episodic subduction arises due to the balancing of driving convective stresses with resistive plate strength. Here we have shown that, for a simplified rheology, a plate tectonic like system will enter an episodic regime for higher mantle heat production. Under the hotter mantle temperatures anticipated for the Precambrian, our models show extremely time-dependent subduction, and this is not only consistent rapid plate velocities at 1.1, 1.9–2.1 and 2.7 Ga, but also with major orogenesis at these times, and major crustal production by both arc-accretion and later plume-volcanism mechanisms.

#### Acknowledgments

This work is supported by the NSF, NASA and a MURF (CO). This is GEMOC publication 499.

#### References

- Aspler, L.B., Chiarenzelli, J.R., 1998. Protracted breakup of Kenorland, a NeoArchean supercontinent? *Sed. Geol.* 120, 75–104.
- Beaumont, C., Jamieson, R.A., Nguyen, M.H., Medvedev, S., 2004. *J. Geophys. Res.* 109. doi:10.1029/2003JB002809.
- Calvert, A.J., Sawyer, E.W., Davis, W.J., Ludden, J., 1995. Archean subduction inferred from seismic images of a mantle suture in the Superior Province. *Nature* 375, 670–674.
- Collerson, K.D., Kamber, B.S., 1999. Evolution of the continents and the atmosphere inferred from Th–U–Nb systematics of the depleted mantle. *Science* 238, 1519–1522.
- Coltice, N., Albarede, F., Gillet, P., 2000. 40K–40Ar constraints on the recycling of the continental crust into the mantle. *Science*, 288, 845–847.
- Condie, K.C., 1998. Episodic continental growth and supercontinents: a mantle avalanche connection? *Earth Plan. Sci. Lett.* 163, 97–108.
- Condie, K., 2003. Incompatible element ratios in oceanic basalts and komatiites: tracking deep mantle sources and continental growth rates with time. *Geochem. Geophys. Geosys.* 4. doi:10.1029/2002GC000333.
- Condie, K., 2004. Supercontinents and superplume events: distinguishing signals in the geologic record. *Phys. Earth Planet. Inter.* 6, 319–332.
- Escartín, J., Hirth, G., Evans, B., 2001. Strength and mode of deformation of partially serpentinized peridotites: implications for the rheology and tectonics of oceanic lithosphere. *Geology* 29 (11), 1023–1026.
- Evans, D.A.D., 2003. True polar wander and supercontinents. *Tectonophysics* 362, 303–320.
- Goldfarb, R.J., Groves, D.I., Gardoll, S., 2001a. Orogenic gold and geologic time: a global synthesis. *Ore Geol. Rev.* 18, 1–75.
- Goldfarb, R.J., Groves, D.I., Gardoll, S., 2001b. Rotund versus skinny orogens: well-nourished or malnourished gold? *Geology* 29, 539–542.
- Griffin, W.L., Doyle, B.J., Ryan, C.G., Pearson, N.J., O'Reilly, S.Y., Davies, R., Kivi, K., Van Achtebergh, E., Natapov, L.M., 1999. Layered mantle lithosphere in the Lac de Gras Area, Slave Craton: composition, structure and origin. *J. Petrol.* 40, 705–727.
- Hall, C.E., Gurnis, M., 2005. Strength of fracture zones from their bathymetric and gravitational evolution. *J. Geophys. Res.* 110. doi:10.1029/2004JB003312.
- Kanamori, H., 1994. Mechanics of earthquakes. *Ann. Rev. Earth Planet. Sci.* 22, 207–237.

- Kemp, A.I.S., Hawkesworth, C.J., Paterson, B.A., Kinny, P.D., 2006. Episodic growth of the Gondwana supercontinent from hafnium and oxygen isotopes in zircon. *Nature* 439, 580–583.
- Kohlstedt, D.L., Evans, B., Mackwell, S.J., 1995. Strength of the lithosphere: constraints imposed by laboratory experiments. *J. Geophys. Res.* 100, 17,587–17,602.
- Lee, C.-T.A., 2006. Geochemical/Petrologic Constraints on the Origin of Cratonic Mantle. In: Benn, K., Mareschal, J.-C., Condie, K.C. (Eds.), *Archean Geodynamics and Environments*, vol. 164. American Geophysical Union Monograph, pp. 89–114.
- McClennan, S.M., Taylor, S.R.J., 1982. Geochemical constraints on the growth of the continental crust. *J. Geol.* 90, 347–361.
- McCulloch, M.T., Bennett, V.C., 1994. Progressive growth of the Earth's continental crust and depleted mantle—geochemical constraints. *Geochim. Cosmochim. Acta* 58, 4717–4738.
- Moresi, L., Solomatov, V.S., 1998. Mantle convection with a brittle lithosphere: thoughts on the global tectonic styles of the Earth and Venus. *Geophys. J. Int.* 133, 669–682.
- Moresi, L., Dufour, F., Mühlhaus, H.-B., 2003. A Lagrangian integration point finite element method for large deformation modeling of viscoelastic geomaterials. *J. Comp. Phys.* 184, 476–497.
- Müller, R.D., Roest, W.R., Royer, J.-Y., Gahagan, L.M., Sclater, J.G., 1997. Digital isochrons of the world's ocean floor. *J. Geophys. Res.* 102, 3211–3214.
- Reese, C.C., Solomatov, V.S., Moresi, L.-N., 1999. Non-Newtonian stagnant lid convection and magmatic resurfacing on Venus. *Icarus* 139, 67–80.
- Reymer, A., Schubert, G., 1984. Continental volume and freeboard through geological time. *Tectonics* 3, 63–67.
- Richards, M.A., Yang, W.-S., Baumgardner, J.R., Bunge, H.-P., 2001. Role of a low-viscosity zone in stabilizing plate tectonics: implications for comparative terrestrial planetology. *Geochem. Geophys. Geosys.* 2. doi:10.1029/2000GC000115.
- Rino, S., Komiya, T., Windley, B.F., Katayama, I., Motoki, A., Hirata, T., 2004. Major episodic increases of continental crustal growth determined from zircon ages of river sands; implications for mantle overturns in the Early Precambrian. *Phys. Earth Planet. Int.* 146, 369–394.
- Simon, L., Lécuyer, C., 2005. Continental recycling: the oxygen isotope point of view. *Geochem. Geophys. Geosys.* 6. doi:10.1029/2005GC000958.
- Snyder, D.B., 2002. Lithospheric growth at margins of cratons. *Tectonophysics* 355, 7–22.
- Stein, M., Hofmann, A.W., 1994. Mantle plumes and episodic crustal growth. *Nature* 372, 63–68.
- Stein, C., Schmalzl, J., Hansen, U., 2004. The effect of rheological parameters on plate behaviour in a self-consistent model of mantle convection. *Phys. Earth Planet. Int.* 142, 2224–2255.
- Tackley, P., 2000. Self-consistent generation of tectonic plates in time-dependent, three-dimensional mantle convection simulations. *Geochem. Geophys. Geosys.* 1 (2000GC000036).
- Taylor, S.R., McLennan, S.M., 1985. *The Continental Crust: its Composition and Evolution*. Blackwell Scientific, Oxford.
- Torsvik, T.H., 2003. The Rodinia jigsaw puzzle. *Science* 300, 1379–1381.
- Turcotte, D.L., 1993. An episodic hypothesis for Venusian tectonics. *J. Geophys. Res.* 98, 17061–17068.
- Turcotte, D.L., Schubert, G., 1982. *Geodynamics: Applications of Continuum Physics to Geological Problems*. John Wiley & Sons, New York. 450 pp.
- van Thienen, P., van den Berg, A.P., Vlaar, N.J., 2004. Production and recycling of oceanic crust in the early Earth. *Tectonophysics*, 386, 41–65.
- Zhong, S., Gurnis, M., Moresi, L., 1998. Role of faults, nonlinear rheology, and viscosity structure in generating plates from instantaneous mantle flow models. *J. Geophys. Res.* 103, 15,255–15,268.